JPL NO. 9950-585

DOE/JPL-955640-81/6

DISTRIBUTION CATEGORY UC-63

DEVELOPMENT AND FABRICATION OF A SOLAR CELL JUNCTION PROCESSING SYSTEM

QUARTERLY PROGRESS REPORT NO. 6

JULY 1981

THE JPL LOW-COST SOLAR ARRAY PROJECT IS SPONSORED BY THE U.S. DEPARTMENT OF ENERGY AND FORMS PART OF THE SOLAR PHOTOVOLTAIC CONVERSION PROGRAM TO INITIATE A MAJOR EFFORT TOWARD THE DEVELOPMENT OF LOW-COST SOLAR ARRAYS. THIS WORK WAS PERFORMED FOR THE JET PROPULSION LABORATORY, CALIFORNIA INSTITUTE OF TECHNOLOGY BY AGREEMENT BETWEEN NASA AND DOE.

PREPARED UNDER CONTRACT NO. 955640 FOR:
JET PROPULSION LABORATORY
CALIFORNIA INSTITUTE OF TECHNOLOGY
PASADENA, CALIFORNIA 91103

spire

DRD No. QR
CDRL Item No. 5

DOE/JPL-955640-81/6
Distribution Category UC-63

DEVELOPMENT AND FABRICATION OF A SOLAR CELL JUNCTION PROCESSING SYSTEM

Report Number QR-10073-06
Quarterly Report

July 1981

This work was performed for the Jet Propulsion Laboratory, California Institute of Technology sponsored by the National Aeronautics and Space Administration under Contract NAS7-100.

Prepared by: _____
Project Engineer

Approved by: _____
Program Manager

SPIRE CORPORATION
Patriots Park
Bedford, MA 01730

TABLE OF CONTENTS

LIST OF FIGURES

SECTION 1
CONTRACT OBJECTIVES

The basic objectives of the program are the following:

1. To design, develop, construct and deliver a junction processing system which will be capable of producing solar cell junctions by means of ion implantation followed by pulsed electron beam annealing.
2. To include in the system a wafer transport mechanism capable of transferring 4-inch-diameter wafers into and out of the vacuum chamber where the ion implantation and pulsed electron beam annealing processes take place.
3. To integrate, test and demonstrate the system prior to its delivery to JPL along with detailed operating and maintenance manuals.
4. To estimate component lifetimes and costs, as necessary for the contract, for the performance of comprehensive analyses in accordance with the Solar Array Manufacturing Industry Costing Standards (SAMICS).

In achieving these objectives, Spire will perform five tasks:

Task 1 - Pulsed Electron Beam Subsystem Development

Task 2 - Wafer Transport System Development

Task 3 - Ion Implanter Development

Task 4 - Junction Processing System Integration

Task 5 - Junction Processing System Cost Analyses

Under this contract the automated junction formation equipment to be developed involves a new system design incorporating a modified, government-owned, JPL-controlled ion implanter into a Spire-developed pulsed electron beam annealer and wafer transport system. Figure 1 presents a conceptual drawing of the junction processing system. When modified, the ion implanter will deliver a 16 mA beam of $^{31}P^{+}$ ions with a fluence of 2.5×10^{15} ions per square centimeter at an energy of 10 keV. The throughput design goal rate for the junction processor is 10^{7} four-inch-diameter wafers per year.

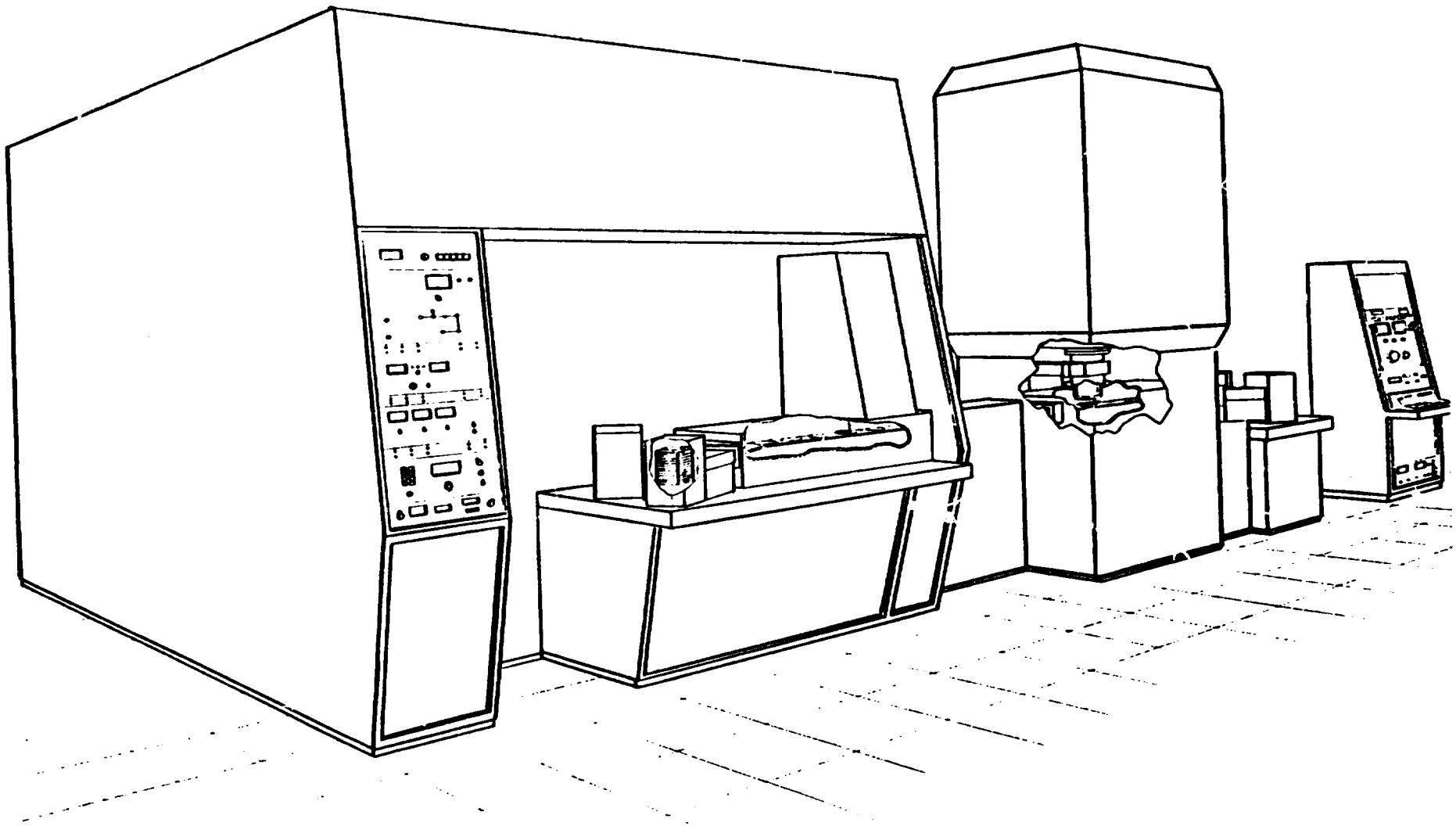

FIGURE 1. SPIRE/JPL JUNCTION PROCESSOR

At the present time, authorization has been given to perform work only on Tasks 1 and 2. The performance of Tasks 3, 4 and 5 has been deferred until a written "Notice to Proceed" with one or more of these deferred tasks is received from JPL.

SECTION 2
SUMMARY OF WORK PERFORMED

2.1 INTRODUCTION

This quarterly report covers the work performed during the period 1 April through 30 June 1981 on Tasks 1 and 2 of a contract for the development and fabrication of a solar cell junction processing system. Assembly and system testing has continued on the Task 1 phase to develop a pulsed electron beam annealing machine. The vacuum chamber fabrication and component procurement for the Task 2 wafer transport system has been ongoing with more than 50 percent of the ordered components received.

2.2 PULSER FABRICATION AND TESTING

Modifications to the ground plane, to insure a good electrical return path during the pulse discharge, were made using a ring of beryllium copper finger stock attached to the underside of the aluminum ground plate.

During this quarter, experiments on annealing of wafers with ion implantation damage continued. The entire surface of 100 mm diameter wafers were annealed by one pulse for the standard implant (10 keV, phosphorus, $2x10^{15}$ ions/cm^2). While samples are being fabricated into solar cells for electrical characterization, work is continuing on improvement of the electron beam uniformity and the optimization of the diode parameters.

2.3 TASK 2 - TRANSPORT DESIGN

The engineering design has been completed and the manufacturing detail drawings were released for fabrication. Assembly of the subcomponents for the exit and entrance locks is almost complete. These components include the cassettes, the indexing mechanisms, main doors and wafer carrier transfer modules. The new "Y" track and three-phase transistion track sections are under final assembly and test and should be operational at the end of July.

SECTION 3
PROGRESS ON TASK 1 - DEVELOPMENT OF PULSED ELECTRON BEAM SUBSYSTEM

3.1 PULSER FABRICATION AND TESTING

3.1.1 Pulse Generator

During the current series of tests, the high voltage power supply, pulse forming lines, switch, and charging resistor were subjected to over 500 cycles at high voltage, mostly 100-160 kV. Modifications required for continuous operation were noted.

The interim high voltage test power supply used is not capable of continuous operation at 2 or 3 second rep-rate at 160 kV. The charging current is low and the safety overload switch trips the supply off after each pulse. A new power supply rated at 300 kV, 17 mA is on order which will have the higher voltage and current capabilities required for the continuous 2 to 3 second rep-rate operation.

The increase in the number of lines in the PFN (Pulse Forming Network) increased the energy stored by 50 percent. This allowed complete annealing of a sample wafer, 100 mm in diameter. However, the increased capacitance (with the existing charging resistor) has an RC time constant of 0.8 seconds — too slow for 2 or 3 $(pps)^{-1}$ operation. The charging resistor must be changed to a lower value, possibly 1/3 lower. This would protect the new power supply while still allowing rapid charging.

The high voltage cable will be replaced. This is consistent with the higher voltage capabilities. Also, the existing cable failed at 180 kV and/or continuous operation at 160 kV.

The high-pressure/high-voltage tank could not operate without occasional flashovers above 160 kV. The flash point is believed to be from the edge of the collection plate (which supports the 12 liners) to the ground plate at the bottom of the tank where it joins the tank walls. An electrical analysis of this structure will be done. Also, the gas mixture in the tank has been changed from pure nitrogen to a mixture of 0.85 N_2, 0.10 CO_2, and 0.05 SF_6. This reduced the arcing considerably. Futher changes may be made.

There are no problems with the switch at the present time. Arc damage in the electrodes is visable but no worse than expected. Operation is smooth and reliable.

3.1.2 Pulse Annealing Tests

Emphasis was placed upon finding the optimum combination of cathode-anode gap, sample-anode distance, cathode radius and magnetic field for annealing high-dose ion implantation damage in silicon. Large scale uniformity of the electron beam (average fluence over distances of approximately 1 cm) was measured with a multi-probe calorimeter. Small scale uniformity of the electron beam (features less than 1 mm) was determined using implanted wafers as witness plates. Results showed that there is a delicate balance between large scale and small scale uniformity when varying the applied magnetic field. Further tests are required for optimum annealing results.

3.1.3 Optimum Geometry

There are three variable distances in the pulse electron beam annealer which affect large scale beam propagation; cathode radius, A-K gap, and sample-anode (S-A) distance. Previous tests (Quarterly Report No. 5) gave a strong indication of acceptable ranges for these parameters.

It was found that complete annealing of a 100 mm wafer, with no area unpulsed near the sample edge, required a cathode at least 4.5 inches in diameter. This is fixed by a slight inward focusing effect on the beam. For larger cathodes (6 inches), uniform focusing of the beam to 100 mm diameter was not possible without altering the magnet pole pieces, which is possible but not necessary at this time. Therefore cathode diameter is judged to be 11.4 cm (4.5 inches) with a 0.32 cm (0.125 inches) radius at the edge.

For this cathode diameter, increasing the A-K gap above 3.0 mm (0.120 inches $\pm$.001) resulted in a higher average electron energy and a longer pulse. It also produced a beam with spotty, non-uniform fluence on a small scale and was not usable. At low A-K gaps the charging voltage required for annealing increased as the pulse duration became shorter. With limitations on the present power supply, experiments were not continued at gaps less than 2.5 mm. Changes in increments of less than 0.5 mm were not considered important for these tests.

The sample-to-anode (S-A) distance was originally set at about 4.5 mm. The area annealed at a variety of conditions was slightly less than the 100 mm circle desired, and the fluence was excessive at the center of the beam. Conditions improved at a spacing of 3.5 mm. Additional experiments were carried out with this

distance as the reference setting. At a S-A distance of 0.8 mm there was severe shadowing by the anode mesh, and the beam focusing could still be detected. No experiments were performed in between 1 and 3.5 mm. The later figure is possibly optimum. At larger S-A distances (6 mm) the beam fluence dropped abruptly.

The anode mesh spacing (0.1 mm wire, 0.85 mm spacing) was fixed by tests on lifetime (see previous Quarterly Report No. 5). A test with 0.05 mm steel wire, 0.4 mm spacing, showed that one arc would rupture the finer mesh. It may still be desirable if random hot spots are eliminated by the use of cleaner processing conditions. The cathode cross-hatch pattern is another variable to be considered.

3.1.4 Magnetic Field Optimization

Optimization of the magnetic field was attempted only after fixing the geometric variables. The calorimeter was used to determine electron beam uniformity as a function of the applied field from 0 to 2.6 kilogauss. The fluence was most uniform, averaged over 0.32 cm^2 areas, at the highest field and generally higher near the center of the beam at low magnetic fields. There was no evidence of "edge" emission from the 4.5 inch cathode at the high magnetic fields as there was from 4 inch cathodes (Quarterly Report No. 5).

3.1.5 Calorimeter

The calorimeter consists of 29 disks arranged in the pattern shown in Figure 2. When irradiated by the electron beam, the disk rises in temperature about 4-6^{o}C and cools slowly with typical time constants exceeding 8 seconds. The disks are within $\pm$5 percent of the average calibration which is corrected for energy radiated away when the surface temperature is very high, right after the pulse. Carbon is the only material which can be used which will not melt or spall from this radiation.

The calorimeter has an electronics package which multiplexes the readout from 25 probes for digitization every 0.5 seconds. The signal from the probes is grounded on one side in three places and filtered to remove RF noise which is destructive to the sensitive amplifier. The digitized signals are analyzed by a microcomputer which extrapolates the temperature profiles to time zero, accounting for average initial readings and the varying delay in the multiplexer. A sample of the corrected data from the computer is shown in Figure 2.

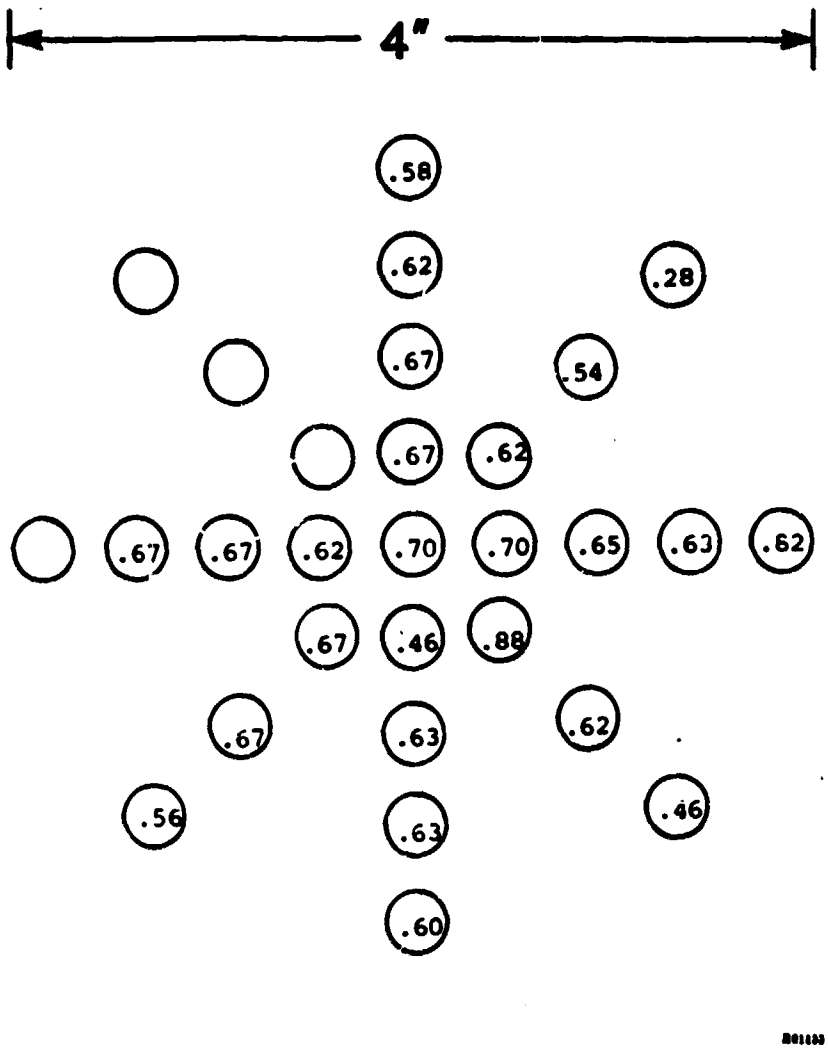

FIGURE 2. CALORIMETER ARRAY AND READOUT

(AVERAGE READING ON ALL POINTS

.64±.09 J/cm²)

3.1.6 Fluence Versus Magnetic Field

The calorimeter array described was used to analyze about 100 shots, which without the automated data analysis becomes an almost impossible task. The cathode-anode gap, sample-anode distance, cathode, and charging voltage were held constant. Readings after initial conditioning, averaged over 3 to 6 probes at each radius and at least two pulses, are shown in Figure 3.

At high magnetic fields, 2.6 kilogauss, the beam extended to 4.5 inch diameter, showing no reduction in intensity outside of the 4 inch circle covered by the calorimeter. At lower values of the applied field, the fluence fell off very sharply beyond a radius of 2 inches. Thus, the total energy in the beam at 2.6 kilogauss was about the same as at lower magnetic field strengths, although the plot in Figure 3 does not extend far enough to show this. There appeared to be some tendency to form a circle of higher fluence at a radius of about 1 inch. This must be checked. However, at high magnetic fields the uniformity shown is acceptable.

3.1.7 Annealing Experiments

Samples for annealing tests were 100 mm diameter silicon wafers with a polished surface and as-cut backs, 0.020 inch thick. They were cleaned, implanted with 2.5×10^{15} ions/cm^2 of 10 keV phosphorus, cleaned a second time and delivered to the junction processor test station. Typical wafer resistivity was 10 ohm-cm. Some samples with etched surfaces, 0.013 inch thick and 1 ohm-cm were tested to see the effect of different wafer parameters. (There were none.) All wafers were annealed in the custom transport carriers designed for the high speed wafer transport system.

These samples showed small-scale non-uniformities (typical spatial variation ~1 mm) which would not show on the calorimeter tests. Briefly, the entire surface of a wafer pulsed at a magnetic field of 1.2 kilogauss was annealed (for other parameters, see previous section). However, there was some surface damage, believed to be slip in the worst case, in the center of the wafer. At a magnetic field of 2.6 kilogauss, the surface was uniformly spotted with small areas of damage adjacent to small areas (~1 mm o.d.) of unannealed meterial. The fine scale variation in the beam fluence was clearly too great.

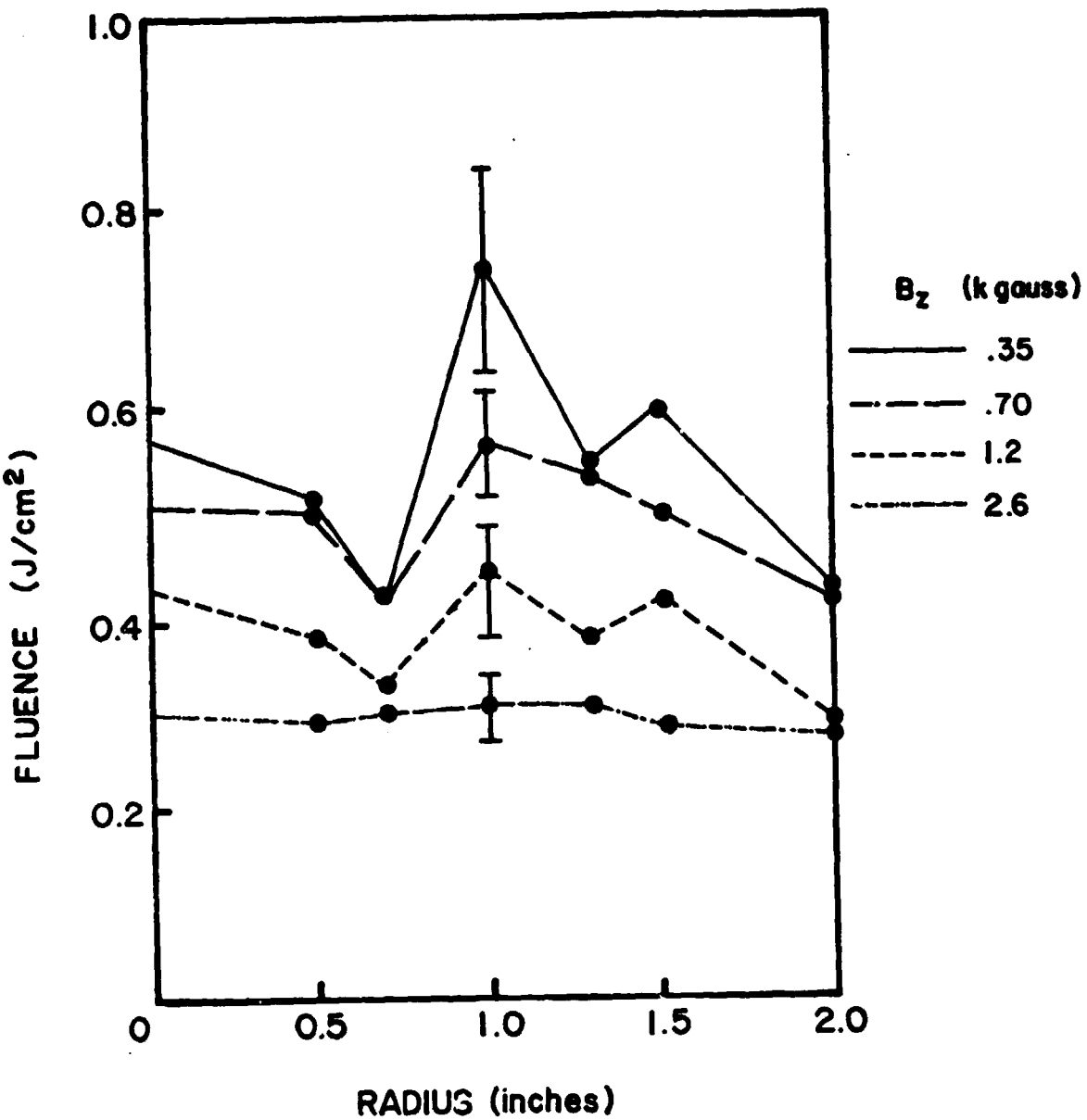

FIGURE 3. AVERAGED CALORIMETER RESULTS

The tests were run at intermediate levels of the applied magnetic field but whenever the large scale variation of the beam was generally acceptable, the fine scale irregularities were not. The fine scale pattern was traceable to the cathode cross-hatch pattern (regular squares, 0.020 inches or 0.5 mm spacing). The next test run will use two approaches: either reduce the fluence at the beam center with acceptable fine scale variations, or reduce the magnitude of these fine scale hot spots by providing more inital emission sites at the cathode.

The physics of the uniformity problem is understood. The electrons are confined to the magnetic field lines at high field strength. This will prevent the beam from pinching due to self-magnetic fields; but also it prevents the electrostatic repulsive forces in the small beamlets from creating the uniform stable beam expected. An optimum combination of cathode design and magnetic field will be determined with additional testing.

3.1.8 Electronic Properties of Test Samples

While solar cells are now being fabricated on pulse annealed wafers, various electronic tests were performed. The sheet resistance of samples with the whole surface annealed is shown in Figure 4, compared to a furnace annealed sample. The lower value for PEBA is consistent with the previous work.[1] It is explained by higher percent activation of the dopant, and by higher electron mobility in the n++ region (resulting from redistribution of the dopant). The junction depth, measured by the groove-and-stain technique on a similar wafer was 0.28 microns, somewhat less than that observed for furnace annealing.

Point probe open-circuit voltage measurements were made on random samples. Initial readings were between 400 to 500 mV. After a thermal cycle of 400°C for 15 minutes, characteristic of a contact sintering step, the values of the open circuit voltage were over 500 mV as measured by the point probe. It was decided to leave further electrical measurements go until after fashioning solar cells.

3.1.9 Electron Beam Characteristics

The diode voltage monitor indicated a significant amount of RF noise for very low impedance diodes at 400 MHz. Because the frequency and amplitude of this signal changed with increasing diode impedance (increased A-K gap or decreased cathode radius) there is the possibility that the signal may represent

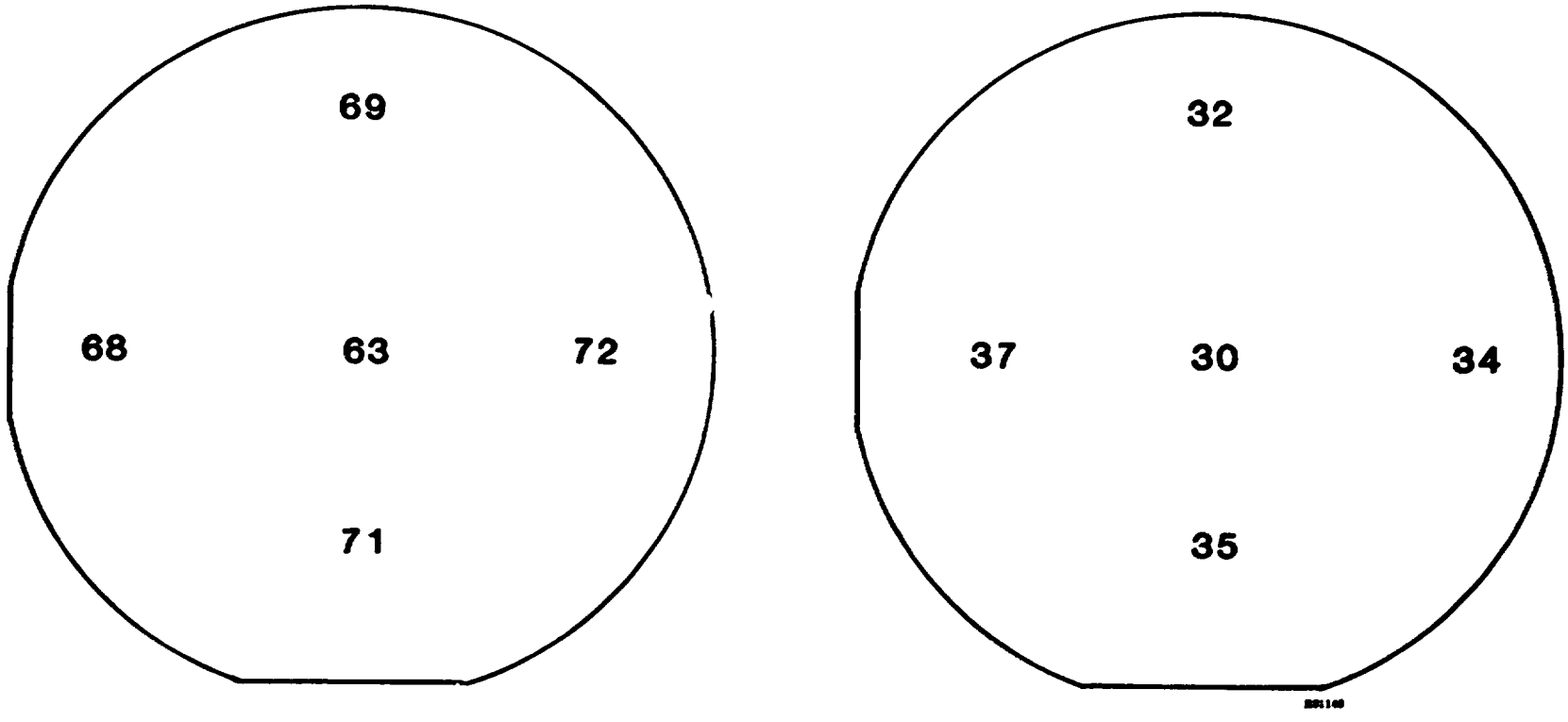

FIGURE 4. SHEET RESISTANCE (ohms/square)

four inch Si wafers
(2×10^{15} $^{31}P^{+}$ / cm^2 @ 10keV)

actual variations in beam energy due to strong plasma oscillations. The frequency is much lower than the cyclotron frequency (approximately 1.76×10^7 times B in gauss) which is over 100 GHz at 2.6 kilogauss. The frequency is closer to the plasma frequency, approximately 10^4 SQRT (electron density), which is 5 GHz at 70 kA for 5 keV electrons. However, since the plasma frequency varies during the pulse and the noise signal frequency does not, there is no simple explanation for the observation. Various ringing frequencies of the coaxial line between the switch and cathode are close to the right value, but do not explain the change seen with different cathodes and gaps unless the reflection of waves change markedly with load impedance. The effect of this signal on annealing is unknown. Although it implies that the diode is an efficienct microwave generator, the change in electron energy and absorbed dose on the sample should not affect heating.

The averaged diode current and voltage characteristics, and calculated electron energy spectra for the annealing conditions used, are shown in Figure 5. The computed absorption of energy versus depth is shown in Figure 6. Because the peak dose is almost twice as large as in previous work,[1] the fluence required for annealing should be lower. This was observed. Current annealing threshold was below 0.5 J/cm^2 (average) compared to 0.9 J/cm^2 reported in earlier studies. This also implies that the melt depth and junction should be more shallow. Early measurements indicate that this might be true. If so, solar cell efficiency from PEBA could be slightly higher than in the previous work.[1]

Annealing the total area of a 100 mm diameter wafer in one pulse has been demonstrated. Additional experiments are required to improve small scale irregularities in the beam. These should be completed by the time the transport system is ready for demonstration.

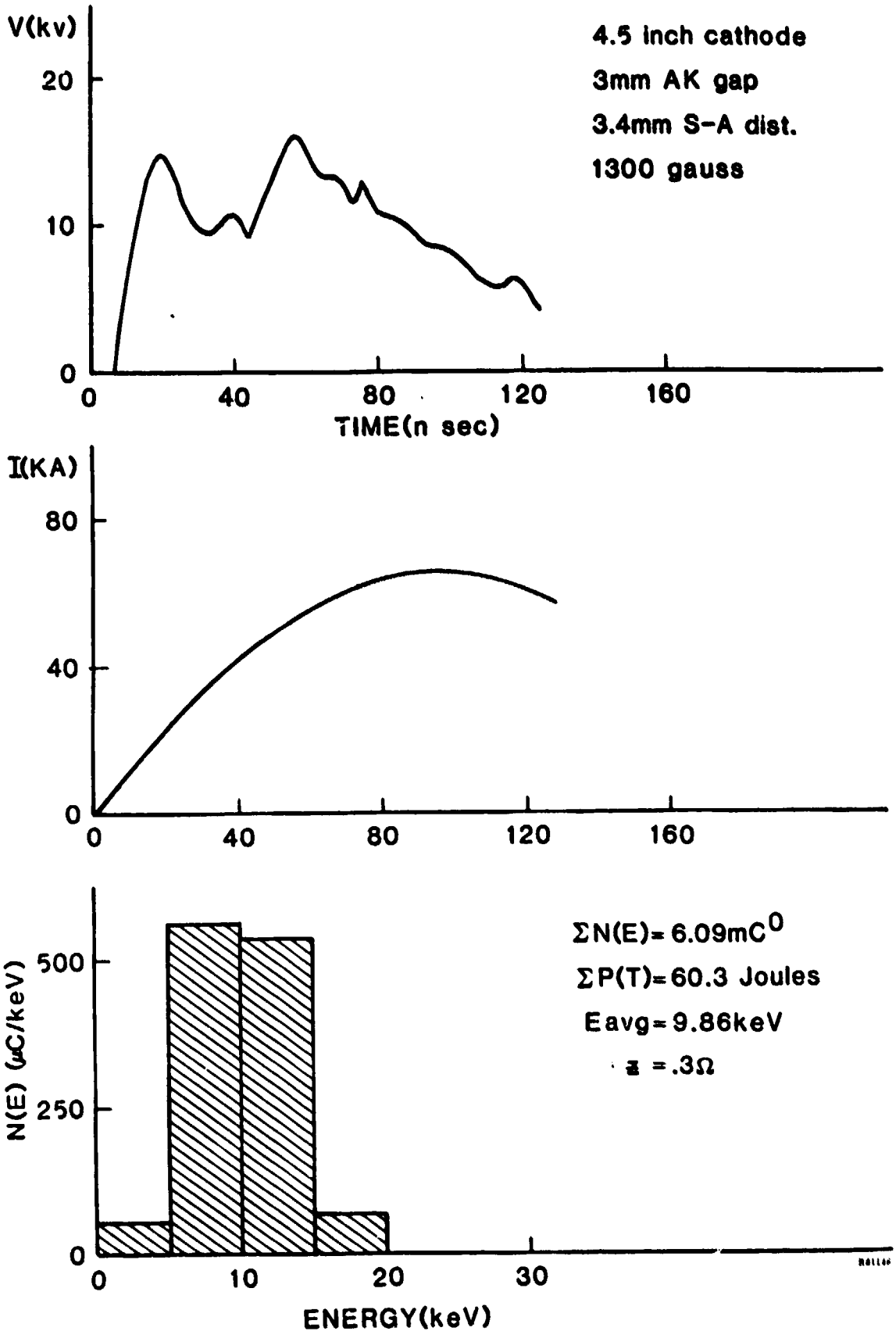

FIGURE 5. SPI-PULSE 7000 DISCHARGE CHARACTERISTICS

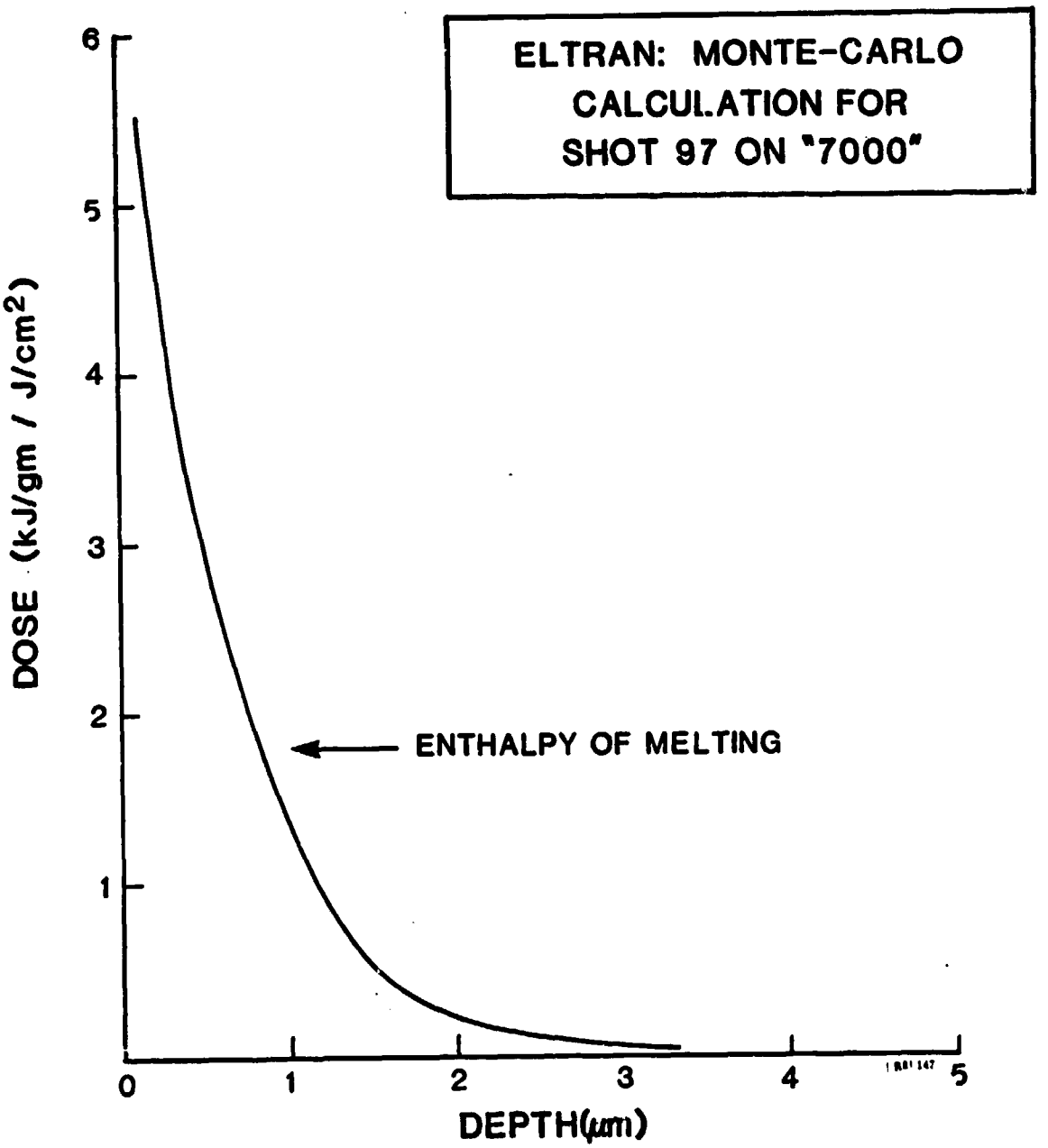

FIGURE 6. ABSORBED ENERGY IN SILICON
(Normalized to 1 J/cm^2 fluence)

SECTION 4
PLANS

During the next reporting period efforts will continue to complete the overall system and test program as previously outlined in Figure 7 with an anticipated demonstration of system performance in August. This demonstration will show the sequential operation of the annealing machine with vacuum wafer transport; all of which will be completely automated under microprocessor control.

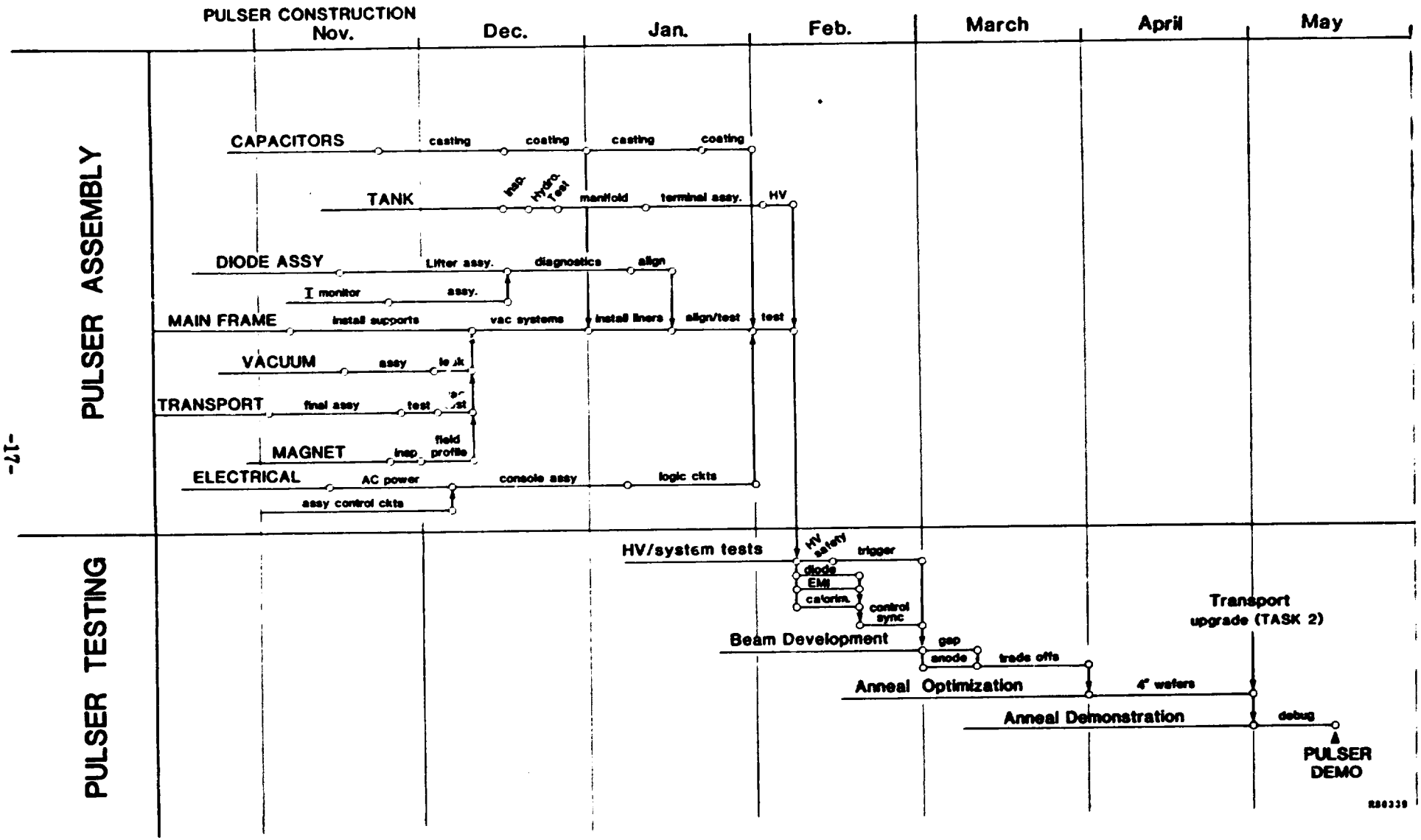

FIGURE 7. SPI-PULSE 7000 ASSEMBLY AND TEST SCHEDULE

SECTION 5
SCHEDULE

Figure 8 shows the projected schedule for Task 1, "Pulsed Electron Beam Subsystem Development".

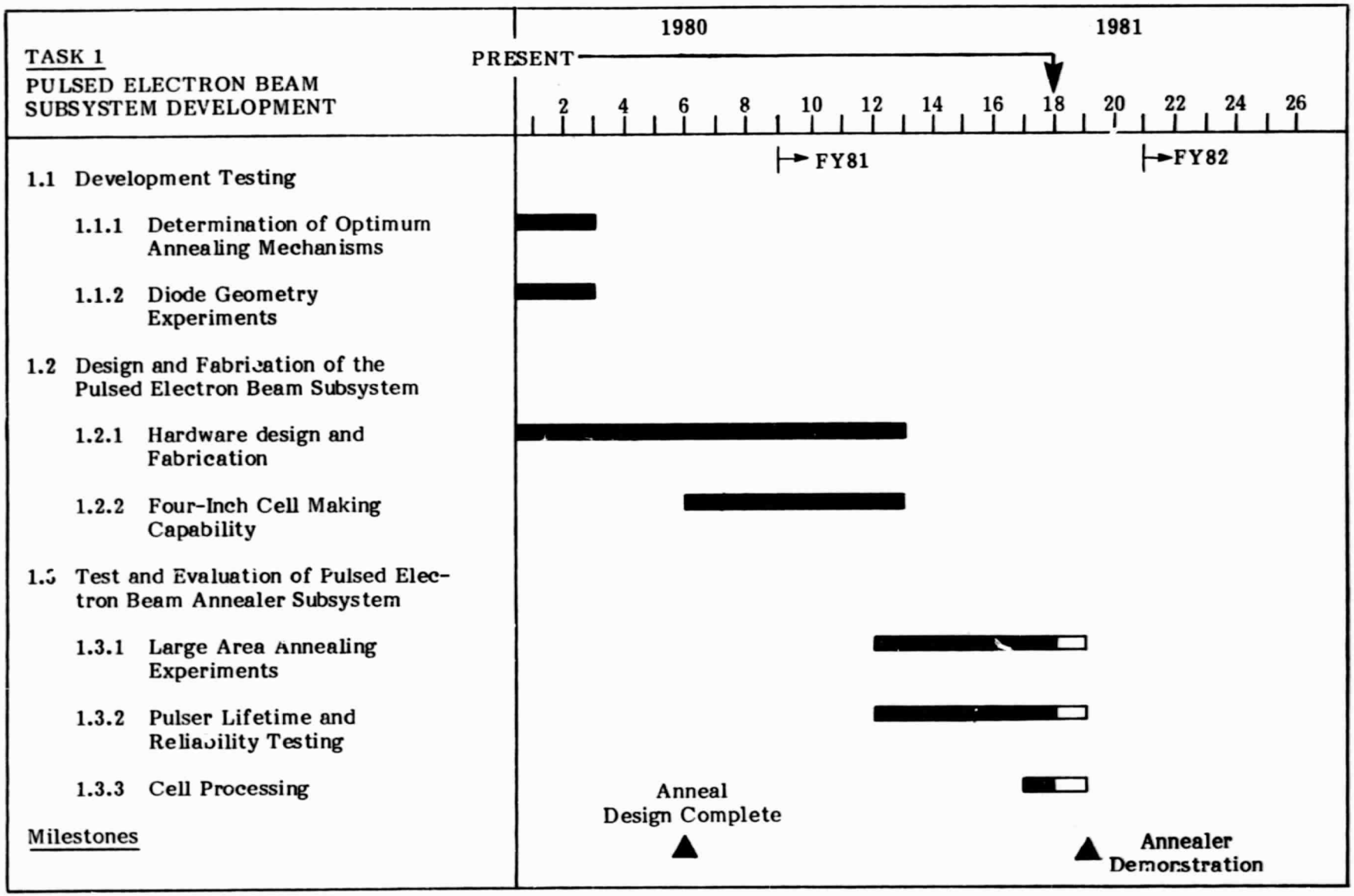

FIGURE 8. TASK 1 SCHEDULE

SECTION 6
PROGRESS ON TASK 2 - WAFER TRANSPORT SYSTEM DEVELOPMENT

6.1 TRANSPORT DESIGN AND FABRICATION

Tests were run on surface coatings for the wafer carriers. Two types of carbon were considered, solid Poco graphite of maximum density and low density Stakfoil™. The former has improved resistance to spallation but is too expensive for many carriers. The latter is inexpensive but cannot take repeated arcing (high fluence) at the same point. Normal beam fluence does not seem to damage either material and a preliminary decision to go with the foil was made. The location (see Figure 9) of the carbon foil segmeted ring, holds the wafer on the carrier and shields the metal parts from the electron beam which must overlap the wafer edge.

The need for a wafer carrier is not yet resolved for the final design. The prototype junction processor will use the carriers to lower wafer temperature during implantation (carrier acts as a heat sink), and to improve current flow during pulsed electron beam annealing. The electron beam current flow is shown in Figure 9. The lifter, which raises the sample from the transport to the firing position, has fingers with 2.5 cm spacing between them (for transport mechanism clearance). Without a carrier, the current flow into the wafer (about 1 kA/cm^2) must move horizontally across this distance through 1-10 ohm cm silicon. This current path would add extra resistance and inductance to the current flow and affect beam homogeniety. With a carrier the current flow through the wafer is vertical. This effect will be evaluated during the next quarter.

The delivery date for the new entrance "Y" track from Brooks Associates has been rescheduled for delivery to Spire in July. The delivery of two of the three-phase transistion track sections have been received and installed in the present PEBA processing station.

The interface control electronics boards have been completed and await integration and test after the arrival of the elevator cassette locks. A layout schematic of the planned transport integration is shown in Figure 10.

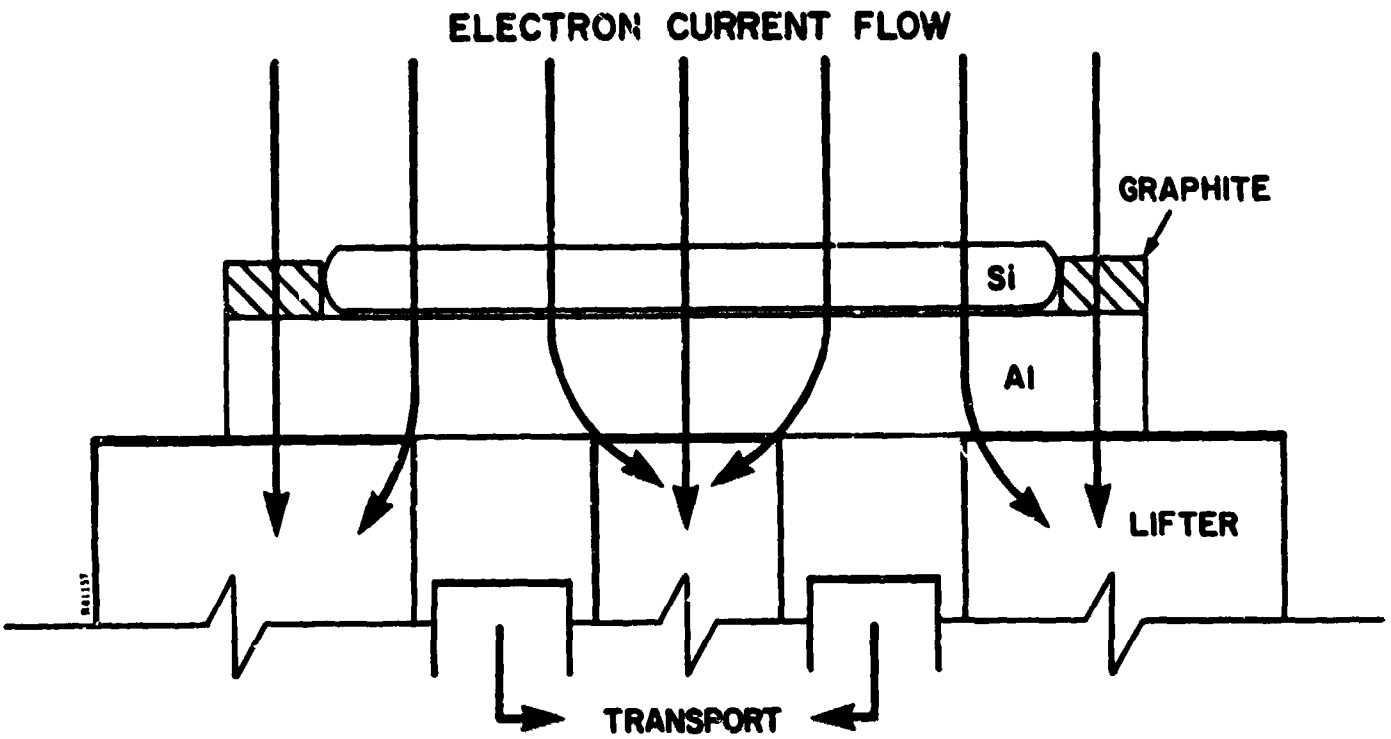

FIGURE 9. WAFER CARRIER, SHOWING CURRENT FLOW DURING PEBA

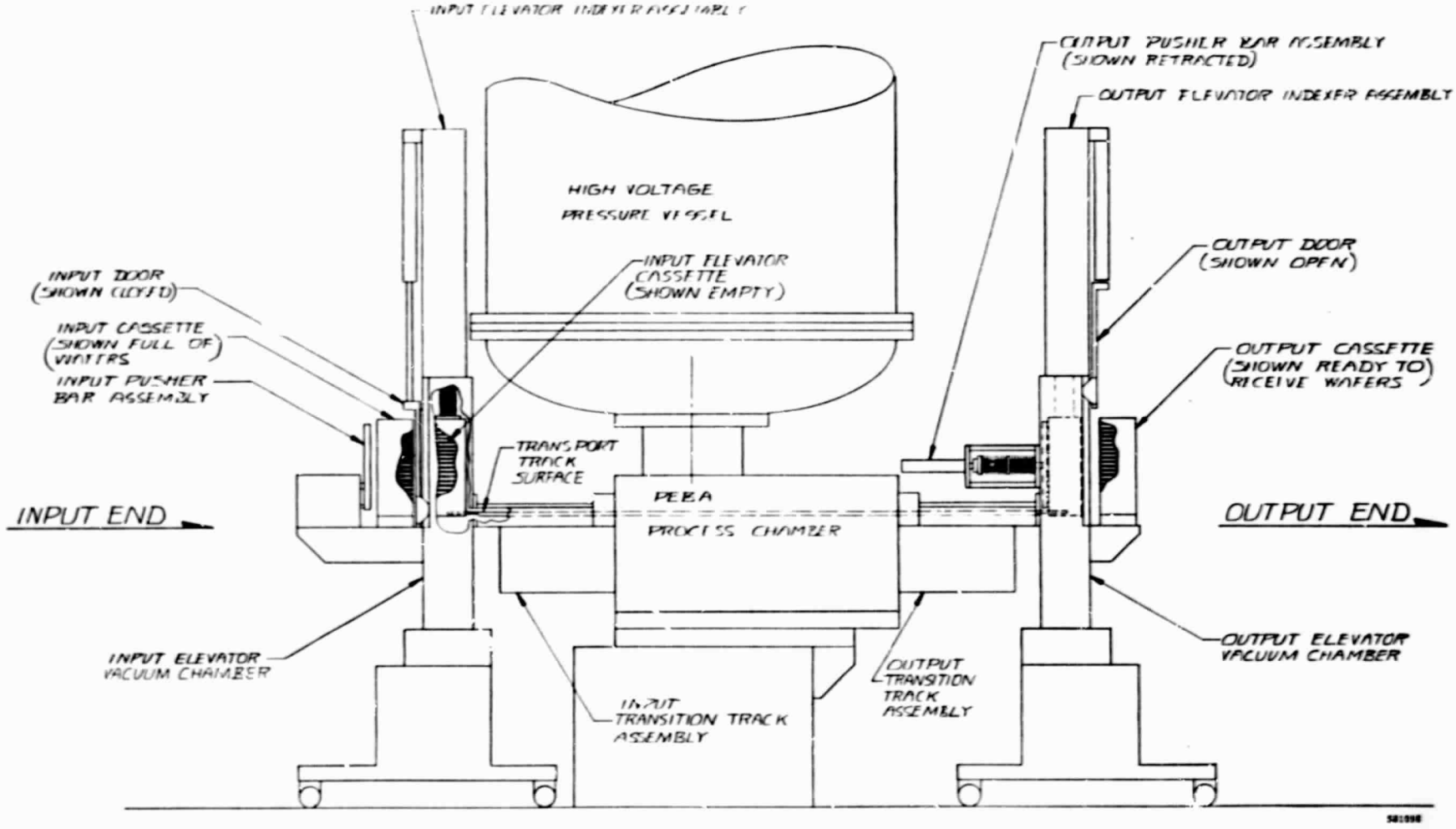

FIGURE 10. SPI-PULSE 7000 ELEVATOR/CHAMBER INTEGRATION

SECTION 7
PLANS

It is anticipated that the vacuum system modifications and the additional hardware and software required to operate the "Y" track transport system will be operational for the system demonstration in the next reporting period.

SECTION 8
SCHEDULE

Figure 11 shows the projected schedule for Task 2 "Wafer Transport System Development".

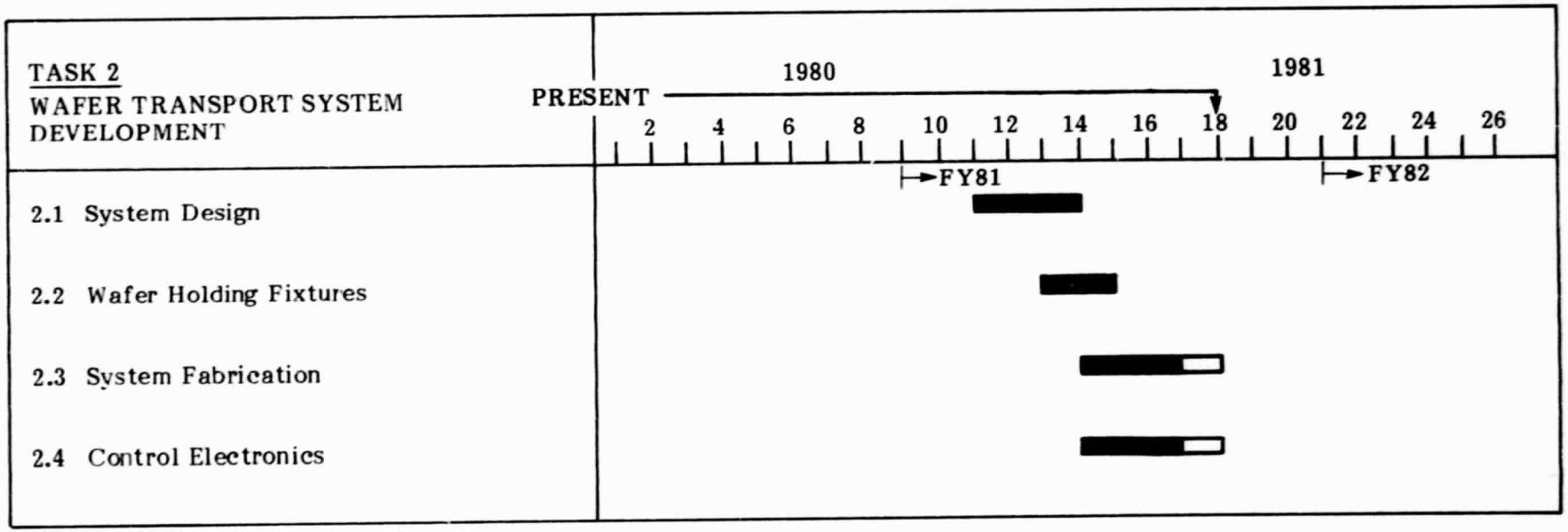

FIGURE 11. TASK 2 SCHEDULE

REFERENCES

1. Spire Corporation, Final Report No. 10052, JPL Contract 954786.